Determination of the density dependence of the nuclear incompressibility

E. Khan[1] and J. Margueron[1,2]

[1]*Institut de Physique Nucléaire, Université Paris-Sud, IN2P3-CNRS, F-91406 Orsay Cedex, France*

[2]*Institut de Physique Nucléaire de Lyon, Université de Lyon 1, IN2P3-CNRS, F-69622 Villeurbanne, France*

(Received 17 April 2013; revised manuscript received 9 September 2013; published 25 September 2013)

Background: The determination of the density dependence of the nuclear incompressibility can be investigated using the isoscalar giant monopole resonance.

Purpose: The importance of the so-called crossing density at subsaturation density is underlined.

Methods: The measurements of the isoscalar giant monopole resonance (GMR), also called the breathing mode, are analyzed with respect to their constraints on the quantity M_c, e.g., the density dependence of the nuclear incompressibility around the so-called crossing density $\rho_c = 0.1$ fm^{-3}.

Results: The correlation between the centroid of the GMR, $E_{\rm GMR}$, and M_c is shown to be more accurate than the one between $E_{\rm GMR}$ and the incompressibility modulus at saturation density, K_∞, giving rise to an improved determination on the nuclear equation of state. The relationship between M_c and K_∞ is given as a function of the skewness parameter Q_∞ associated with the density dependence of the equation of state. The large variation of Q_∞ among different energy density functionals directly impacts the knowledge of K_∞: A better knowledge of Q_∞ is required to deduce more accurately K_∞. Using the local density approximation, a simple and accurate expression relating $E_{\rm GMR}$ and the quantity M_c is derived and successfully compared to the fully microscopic predictions.

Conclusions: The measurement of the GMR constrains the slope of the incompressibility M_c at the crossing density rather than the incompressibility modulus at the saturation density.

DOI: 10.1103/PhysRevC.88.034319 PACS number(s): 21.65.−f, 21.10.Re, 21.60.Jz, 24.30.Cz

I. INTRODUCTION

The determination of the nuclear incompressibility is a longstanding problem. The earliest microscopic analysis came to a value of $K_\infty = 210$ MeV [1], but with the advent of microscopic relativistic approaches, a value of $K_\infty = 260$ MeV was obtained [2]. The fact that K_∞ cannot be better determined than 230 ± 40 MeV, taking into account the whole data on the isoscalar giant monopole resonance (GMR), as well as the various methods to relate the GMR to K_∞ (see, e.g., Refs. [1–9]), leads to a recent effort to reanalyze the method [10].

Pairing effects and similarly the shell structure effects on the nuclear incompressibility were analyzed along these lines. Since the first investigation [11], several studies have shown that pairing effects have an impact on the determination of K_∞ [7,8], and it was considered as a possible cause of the difficulty to accurately constrain K_∞. This effect of pairing on the incompressibility modulus has also been analyzed in nuclear matter, showing that the main effect is occurring at subsaturation densities [12]. However, there is a general consensus between the various microscopic models that pairing effects on K_∞ are not strong enough to explain the lack of accuracy in the determination of the nuclear incompressibility [7–9,13]. Other effects have to be investigated.

Recently, the density dependence of the nuclear incompressibility was reinvestigated, suggesting that the correlation between the centroid of the GMR and the incompressibility modulus K_∞ at saturation density is blurred by the density dependence of the nuclear equation of state in different models [10]. The observed differences in the extraction of K_∞ from the energy of the GMR ($E_{\rm GMR}$) are based on different models and attributed to the density dependence of the equation of state (EoS), which has still to be better constrained. The observation of a crossing point provided a possible path to be investigated. The crossing point arises from energy density functionals (EDFs) that are designed to describe finite-nuclei observables: Their density-dependent incompressibility $K(\rho)$ crosses around the mean density in nuclei, $\rho_c \simeq 0.1$ fm^{-3}. It was therefore proposed that the quantity M_c, e.g., the density dependence of $K(\rho)$ around the crossing density ρ_c, is the quantity that shall be constrained by measurements of the GMR instead of K_∞.

The aim of the present article is to further analyze the correlation method from which is extracted the incompressibility modulus K_∞ and to give a better basis on the alternative method based on the correlation between $E_{\rm GMR}$ and M_c. A comparison between the two methods is given in Sec. II for ^{208}Pb and ^{120}Sn nuclei, showing the relevance of the new method [10]. In Sec. III the source of uncertainties in the determination of K_∞ is directly related to the skewness parameter Q_∞. The skewness parameter gives a contribution to the limitation on the knowledge of the density dependence of the nuclear EoS between the crossing and the saturation densities. The origin of the crossing density is also demonstrated in the case of the Skyrme and Gogny EDFs. In Sec. IV, the explicit relation between the centroid of the GMR and the quantity M_c is derived using the local density approximation (LDA) and keeping as much as possible analytical relations between the various quantities to facilitate their interpretation. The results are compared to the fully microscopic one. Conclusions are given in Sec. V.

II. THE MICROSCOPIC APPROACH

In this section, we first summarize the constrained Hartree-Fock-Bogoliubov (CHFB) approach used to accurately predict the isoscalar GMR energy. We then provide the definition

of the parameter M_c, driving the density dependence of the incompressibility around the crossing point. Finally, using these two quantities, the correlation analysis between the GMR energy and the incompressibility modulus K_∞ on one hand and the GMR energy and the parameter M_c at the crossing density on the other hand are compared.

A. Microscopic calculation of the GMR energy

We first recall how to evaluate the energy of the GMR. We use the sum rule approach to microscopically calculate the centroid energy of the GMR. In such a microscopic approach, we calculate the energy as

$$E_{\rm GMR} = \sqrt{\frac{m_1}{m_{-1}}}, \tag{1}$$

where the kth energy-weighted sum rule is defined as

$$m_k = \sum_i (E_i)^k |\langle i|\hat{Q}|0\rangle|^2, \tag{2}$$

with the RPA excitation energy E_i and the isoscalar monopole transition operator,

$$\hat{Q} = \sum_{i=1}^{A} r_i^2. \tag{3}$$

The calculations using fully microscopic approaches based on EDF are usually performed using the CHFB or the RPA approach [14]. In the present case we calculate the GMR centroid for the Skyrme EDF with the CHFB approach. For completeness, results using other functionals such as Gogny and relativistic functionals are also given. The CHFB method is known to provide an accurate prediction of the GMR centroid.

In the following the energy-weighted moment m_1 and the m_{-1} moment are directly evaluated from the ground state obtained from Skyrme CHFB calculations. The moment m_1 is evaluated by the double commutator using the Thouless theorem [15],

$$m_1 = \frac{2\hbar^2 A}{m}\langle r^2\rangle, \tag{4}$$

where A is the number of nucleons, m is the nucleon mass, and $\langle r^2\rangle$ is the rms radius evaluated on the ground-state density given by Skyrme HFB.

Concerning the evaluation of the moment m_{-1}, the constrained HFB approach is used. It should be noted that the extension of the constrained HF method [4,16] to the CHFB case has been demonstrated in Ref. [17] and employed in Ref. [8]. The CHFB Hamiltonian is built by adding the constraint associated with the isoscalar monopole operator, namely,

$$\hat{H}_{\rm constr.} = \hat{H} + \lambda\hat{Q}, \tag{5}$$

and the m_{-1} moment is obtained from the derivative of the expectation value of the monopole operator on the CHFB solution $|\lambda\rangle$,

$$m_{-1} = -\frac{1}{2}\left[\frac{\partial}{\partial\lambda}\langle\lambda|\hat{Q}|\lambda\rangle\right]_{\lambda=0}. \tag{6}$$

B. Constraints on the equation of state deduced from $E_{\rm GMR}$

Next, the parameter M_c is defined. Instead of correlating $E_{\rm GMR}$ and K_∞, it was proposed that the energy of the GMR (1) gives a strong constraint on the quantity M_c defined, at the crossing density $\rho_c \simeq 0.1$ fm^{-3}, as [10]

$$M_c \equiv 3\rho_c K'(\rho)|_{\rho=\rho_c}, \tag{7}$$

where the density-dependent incompressibility $K(\rho)$ is derived from the thermodynamical compressibility $\chi(\rho)$ as [18]

$$K(\rho) = \frac{9\rho}{\chi(\rho)} = \frac{18}{\rho}P(\rho) + 9\rho^2\frac{\partial^2 E(\rho)/A}{\partial\rho^2}, \tag{8}$$

and the pressure is

$$P(\rho) \equiv \rho^2\frac{\partial E(\rho)/A}{\partial\rho}. \tag{9}$$

The parameter M_c was introduced instead of $K_\infty \equiv K(\rho_0)$ (where ρ_0 is the saturation density) in the correlation analysis based on $E_{\rm GMR}$ because (i) the crossing density ρ_c is closer to the average density in finite nuclei than the saturation density ρ_0 and (ii) the crossing of the incompressibility at ρ_c makes $E_{\rm GMR}$ mostly sensitive to the derivative of the incompressibility at the crossing density [10]. It should be noted that the existence of a crossing density for other EoS quantities, such as, for instance, the symmetry energy [19], the neutron EoS [20,21], and the pairing gap in nuclear matter [22], was also observed. It might reveal the general trend that the experimental constraints drive these quantities towards a crossing point at around the average density of finite nuclei. Various EDFs shall, however, exhibit various density dependencies around the crossing point. At first order the derivative of the incompressibility (or symmetry energy or pairing gap) at this point will differ between various EDFs and additional measurements in nuclei shall characterize these derivatives. For instance, the derivative of the neutron EoS around $\rho_c \simeq 0.11$ fm^{-3} was found to be strongly correlated to the neutron skin in ^{208}Pb [20,21], giving a strong support to improved experimental measurements of this quantity [23].

Figure 1 depicts $K(\rho)$, between half of the saturation density and the saturation density, for several Gogny, Skyrme, and relativistic EDFs. A large dispersion is observed at saturation density ($\rho/\rho_0 = 1$), whereas at $\rho/\rho_0 \simeq 0.71$ there is a much more focused area, defining the crossing density ρ_c.

For several EDFs, Table I displays $K_c \equiv K(\rho_c)$ and K_∞, the values of the incompressibility modulus defined, respectively, at the crossing density $\rho_c = 0.71\rho_0$ and at the saturation density. As also noted on Fig. 1, the Skyrme EDF have a similar density dependence (see the discussion in Sec. III B). The dispersion of K_c values is increased considering relativistic EDFs, because of the various density dependencies among these EDFs. It is therefore more a crossing band that is observed around the crossing density than a crossing point. Considering all the EDFs, the standard deviation is 5.2 MeV on K_c, to be compared with 24 MeV on K_∞. The very weak dispersion in absolute value of K_c as a function of the EDFs is striking, whereas the incompressibility modulus at the saturation density K_∞ is more scattered.

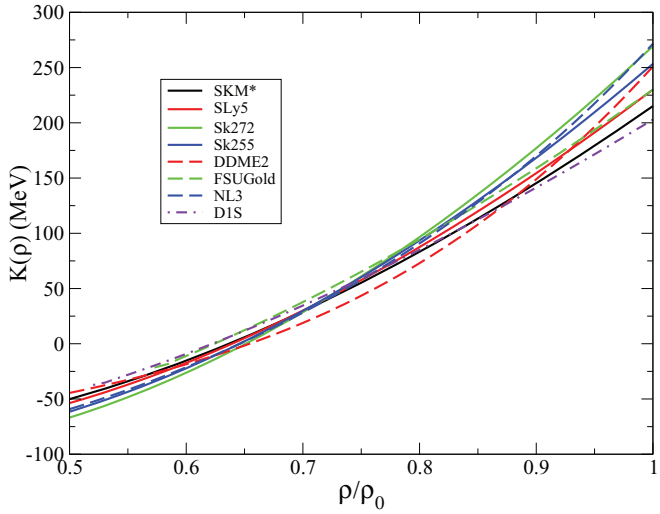

FIG. 1. (Color online) EoS incompressibility $K(\rho)$ calculated with various relativistic and nonrelativistic functionals. The Skyrme EDFs are in solid lines.

To investigate the origins of this weak dispersion of K_c, we now analyze the two contributions to the density-dependent incompressibility, as depicted by Eq. (8). The first term of the right-hand side in Eq. (8) is proportional to the pressure $P(\rho)$, which is indeed related to the first derivative of E/A and the second term is the second derivative of the binding energy E/A with respect to the density. The former vanishes at saturation density, by definition, and K_∞ is related only to the second derivative of the binding energy, $K_\infty = 9\rho_0^2 \frac{\partial^2 E(\rho)/A}{\partial \rho^2}|_{\rho_0}$. Table II displays the expectation values of these two contributions to the incompressibility at the crossing density K_c and for the Skyrme EDFs. The first and second derivatives of the energy per particle E/A act in opposite signs. The contribution of the pressure at ρ_c is not negligible, at variance with its contribution at ρ_0, and largely contributes to the stabilization of K_c. The correlations between $E_{\rm GMR}$ and the solely second derivative of E/A at the saturation density might not be the most appropriate one and the EDF-invariant property of the crossing point (ρ_c, K_c) shall be useful.

TABLE I. Values of K_c and K_∞: Incompressibility $K(\rho)$ at crossing ($\rho_c = 0.71\rho_0$) and saturation densities, respectively. The mean value and the standard deviation are displayed on the two last lines.

EDFs	Crossing K_c (MeV)	Saturation K_∞ (MeV)
SLy5	36	230
SkM*	34	217
Sk255	36	255
Sk272	35	272
SGII	34	215
D1S	38	210
NL3	33	271
DDME2	22	251
FSUGold	41	229
Mean	34.3	238.9
Standard deviation	5.2	24.0

TABLE II. Evaluation of K_c and of the two terms defining the incompressibility $K(\rho)$ [Eq. (8)] at the crossing density $\rho_c = 0.71\rho_0$ for a set of different Skyrme EDFs.

EDFs	Crossing		
	K_c (MeV)	$\frac{18}{\rho_c} P(\rho_c)$ (MeV)	$9\rho_c^2 \frac{\partial^2 E(\rho)/A}{\partial \rho^2}|_{\rho_c}$ (MeV)
SLy5	36	−103	139
SkM*	34	−99	133
Sk255	36	−113	149
Sk272	35	−119	154
SGII	34	−98	132

C. $(E_{\rm GMR}, K_\infty)$ versus $(E_{\rm GMR}, M_c)$ correlation analysis

Using $E_{\rm GMR}$ and M_c discussed in the previous sections, it is possible to determine if M_c is better constrained by $E_{\rm GMR}$ than K_∞. The correlation diagrams $(E_{\rm GMR}, M_c)$ and $(E_{\rm GMR}, K_\infty)$ are compared on Figs. 2 and 3, respectively. Two nuclei are considered: the doubly magic ^{208}Pb and the semimagic ^{120}Sn nuclei. In this latter case, pairing effects are known to slightly impact the position of the GMR [12], leading to a larger dispersion compared to the ^{208}Pb case. In the ^{208}Pb case, the $(E_{\rm GMR}, M_c)$ correlation is well pronounced: A correlation coefficient close to one ($r = 0.94$) is obtained. The $(E_{\rm GMR}, K_\infty)$ correlation displays a weaker correlation coefficient ($r = 0.79$). Similar conclusions can be drawn on ^{120}Sn; namely, M_c is a better correlated quantity with $E_{\rm GMR}$ than K_∞. In this nucleus, the correlation coefficients are weaker than in ^{208}Pb because of pairing effects which spread a bit more the GMR predictions. It is rather delicate to deduce an accurate value of K_∞ from GMR measurements in ^{120}Sn because of the weak correlation on $(E_{\rm GMR}, K_\infty)$. In

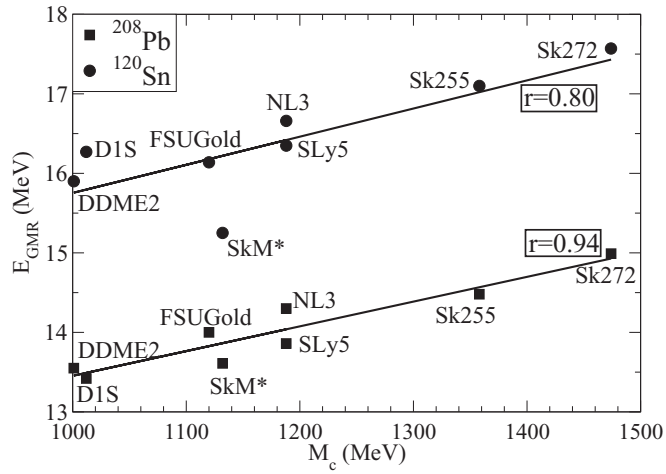

FIG. 2. Centroid of the GMR in ^{208}Pb and ^{120}Sn calculated with the microscopic method (see text) vs the value of M_c for various functionals [3,5,10,24–29]. The solid lines correspond to linear regression for each nuclei. The corresponding correlation coefficient r is displayed.

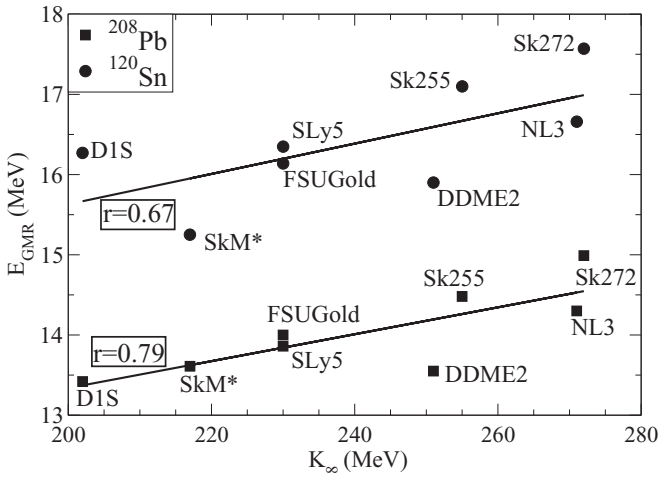

FIG. 3. Same as Fig. 2 with K_∞.

summary, considering various models with different density dependencies and two different nuclei, a better correlation is observed between $E_{\rm GMR}$ and M_c, compared to the one between $E_{\rm GMR}$ and K_∞. It should be noted that these considerations on the slope of the incompressibility M_c at the crossing point have recently been used in Ref. [24], where a good linear correlation between $E_{\rm GMR}$ and M_c is also found, including the so-called BCPM functional.

In more detail, it should be noted that the relativistic DDME2 interaction in the correlation graph ($E_{\rm GMR}$,K_∞) is largely deviating from the others, as it is well known [2–4], while it is much more compatible with the others in the graph ($E_{\rm GMR}$,M_c) [10]. On the contrary, restricting to the Skyrme interactions, the quantities ($E_{\rm GMR}$,K_∞) and ($E_{\rm GMR}$,M_c) are similarly well correlated. This is directly related to the good correlation between (M_c,K_∞) owing to a similar density dependence among the Skyrme EDFs (in ρ^α), which is discussed in Sec. III C.

These results on M_c provide a step towards compatible results between Skyrme, Gogny, and relativistic approaches [10]. The extracted value for the quantity M_c in ^{120}Sn and ^{208}Pb nuclei are also in better agreement between each other than the corresponding K_∞ values: Considering the various EDFs as well as the ^{120}Sn and the ^{208}Pb data, one gets $M_c \simeq 1050 \pm 100$ MeV (9% uncertainty), and $K_\infty \simeq 230 \pm 40$ MeV (17% uncertainty) [10]. The value of M_c and its error bar are deduced from the measurement of the GMR, intersecting the linear fits on correlation plots such as Figs. 2 and 3, on a dozen nuclei (see Fig. 3 of Ref. [10] and text therein). The value of K_∞ and its error bar are deduced from the crossing area on Fig. 1 and the observed spreading of K_∞ at saturation densities [10].

In summary, using microscopic approaches, it is observed that the correlation between M_c and the centroid $E_{\rm GMR}$ is less dispersive and therefore more universal among various models, than the one between K_∞ and $E_{\rm GMR}$ [10]. In the next section we provide a more quantitative understanding of the differences between the quantities M_c and K_∞, explaining the role of the density dependence of the EoS between the crossing and the saturation densities.

III. DENSITY EXPANSION OF THE EQUATION OF STATE

The striking stability of K_c among the various Skyrme EDFs (Table I) deserves an investigation. In this section, the density dependence of the EoS is discussed in terms of the derivatives of the EoS with respect to the density. The stability of K_c as well as the relation between the slope of the incompressibility modulus M_c and the parameters K_∞ and Q_∞ are derived, providing an explanation for the difficulty to constrain K_∞.

A. Density dependence of the equation of state around ρ_0

We start from a systematic expansion around the saturation density ρ_0 of the binding energy, such as in the generalized liquid drop model (GLDM) [30,31], where, in symmetric matter, the energy per particle reads

$$E(x) = E_\infty + \tfrac{1}{2}K_\infty x^2 + \tfrac{1}{6}Q_\infty x^3 \cdots, \qquad (10)$$

with $x = (\rho - \rho_0)/(3\rho_0)$, ρ_0 being the saturation density of symmetric nuclear matter. Q_∞ is the third derivative of the energy per particle.

Applying Eqs. (8) and (9) to the expansion Eq. (10), one obtains the pressure,

$$P(x) = \tfrac{1}{3}(1+3x)^2\left[K_\infty x + \tfrac{1}{2}Q_\infty x^2 + \cdots\right], \qquad (11)$$

and the incompressibility,

$$K(x) = (1+3x)[K_\infty + (9K_\infty + Q_\infty)x + 6Q_\infty x^2 + \cdots]. \qquad (12)$$

Figure 4 displays the binding energy Eq. (10), pressure Eq. (11), and incompressibility Eq. (12) as function of the

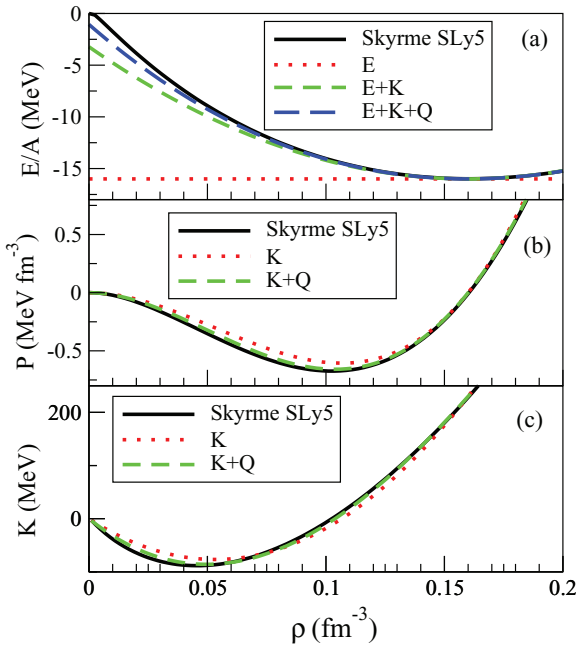

FIG. 4. (Color online) (a) Binding energy E/A in MeV, (b) pressure in MeV fm^{-3}, and (c) incompressibility K in MeV, as functions of the density for various truncation in the expansion Eq. (10). See text for more details.

TABLE III. Parameters appearing in the density expansion of the binding energy E/A Eq. (10) for a set of models considered in this work: ρ_0 is the saturation density, E_∞ the binding energy, K_∞ the incompressibility modulus, and Q_∞ the skewness parameter.

	ρ_0 (fm^{-3})	E_∞ (MeV)	K_∞ (MeV)	Q_∞ (MeV)
SLy5	0.160	−15.98	230	−363
SkM*	0.160	−15.79	217	−386
Sk255	0.157	−16.35	255	−350
Sk272	0.155	−16.29	272	−306
D1S	0.163	−16.02	210	−596
NL3	0.148	−16.24	271	189
DDME2	0.152	−16.14	251	478
FSUGold	0.148	−16.30	229	−537

density ρ going from 0 to 0.2 fm^{-3}, which correspond to the SLy5 Skyrme parametrization [29]. Apart for the solid lines that are obtained from the full Skyrme interaction, the other curves correspond to various approximations in the density expansion of the binding energy [Eq. (10)]. For instance, the dotted line in the binding energy E/A corresponds to the 0th order in the density expansion where only the quantity E_∞ has been included, all other quantities being set to zero. The dashed line $(E + K)$ takes into account the quantities E_∞ and K_∞, and the long-dashed line $(E + K + Q)$ includes the quantities E_∞, K_∞, and Q_∞. Similar approximations have been performed in the case of the pressure [Eq. (11)] and incompressibility [Eq. (12)]. A good convergence towards the full Skyrme interaction is found when successively including in the expressions for the binding energy, the pressure, and the incompressibility the quantities E_∞, K_∞, and Q_∞. These quantities can therefore reasonably well describe the density dependence of the EoS and are given in Table III for a set of models considered in this work.

It is clear from Table III that while the quantities E_∞ and K_∞ are not varying by more than 20%, the values for the skewness parameter Q_∞ are almost unconstrained and can vary by more than 100% among the models. The uncertainty in the determination of the skewness parameter Q_∞ gives, in a quantitative way, the main lack of knowledge in the density dependence of the EoS. The uncertainty on Q_∞ also impacts the density dependence of the pressure and, more interestingly here, of the incompressibility.

B. Stability of K_c

Let us now provide an explanation for the stability of K_c observed in Table III. From Eq. (12), and assuming the validity of a density expansion from ρ_0 to ρ_c, we obtain

$$K_c \simeq (1 + 3x_c)[(1 + 9x_c)K_\infty + (1 + 6x_c)x_c Q_\infty], \quad (13)$$

with $x_c \equiv (\rho_c - \rho_0)/(3\rho_0)$.

In the case of Skyrme interaction, there is a good correlation among the quantities K_∞ and Q_∞, as shown in Fig. 5. The parameters K_∞ and Q_∞ are mostly determined by the same term, the term t_3 in ρ^α, in the case of Skyrme interaction [10]. Owing to their similar density dependence (in ρ^α), the Skyrme EDFs exhibit indeed a linear correlation among these two quantities, whereas the picture is blurred when considering

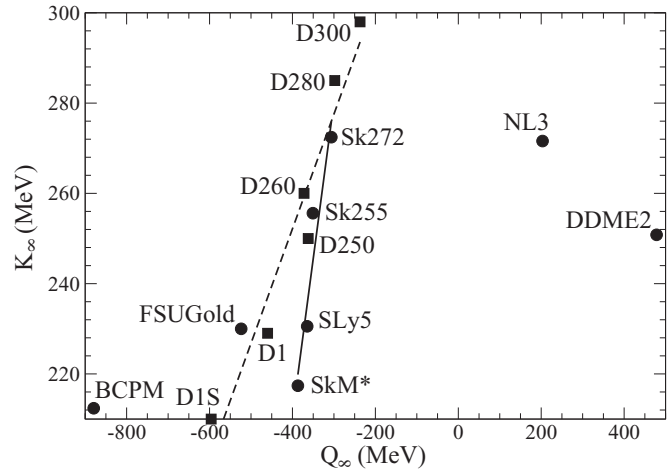

FIG. 5. K_∞ versus Q_∞ for several models. The solid and dashed lines correspond to the fit on the Skyrme and Gogny EDFs values, respectively.

at the same time Skyrme and relativistic EDFs. A linear correlation is also found in the Gogny EDFs case on Fig. 5, which have a similar t_3 in ρ^α density dependence [32]. This confirms that the (K_∞, Q_∞) correlation emerges because of the t_3 term of these EDFs. On the contrary, we have checked that there is not such a correlation among the relativistic NL2, NL3, TM1, TM2, and NL-SH EDF families, having no t_3 term [25].

The linear correlation among the Skyrme and Gogny EDFs can be described by

$$K_\infty = a + bQ_\infty, \quad (14)$$

with $a = 338 \pm 9$ MeV and $b = 0.29 \pm 0.03$ for the Skyrme EDFs and $a = 354 \pm 8$ MeV and $b = 0.25 \pm 0.04$ for the Gogny ones. Injecting Eq. (14) into Eq. (13), one gets

$$K_c \simeq (1 + 3x_c)[(1 + 9x_c)a + f(x_c)Q_\infty], \quad (15)$$

with $f(x) = [6x^2 + (9b + 1)x + b]$. An EDF-almost-independent value of K_c is therefore obtained for $f(x) = 0$ because Q_∞ is the only EDF-dependent quantity in Eq. (15): The solution of $f(x) = 0$ therefore provides the crossing point observed on Fig. 1. The function $f(x)$ has only one zero for positive densities, given by $x_c = -0.095 \pm 0.002$ for Skyrme EDFs and $x_c = -0.093 \pm 0.002$ for Gogny ones, which corresponds to $\rho = (0.714 \pm 0.005)\rho_0 \equiv \rho_c$ for Skyrme EDFs and $\rho = (0.721 \pm 0.005)\rho_0 \equiv \rho_c$ for Gogny ones.

It is interesting to notice that the values for x_c obtained for Skyrme and Gogny EDFs are close to $-1/9$, for which $\partial f/\partial b = 0$. This fact provides an explanation of the weak dependence of the crossing point on the correlation pattern (the value of the coefficient b).

In summary, for the Skyrme and Gogny EDFs there is therefore a density, ρ_c, for which the incompressibility modulus $K(\rho_c)$ is independent from the quantities K_∞ and Q_∞ defined in Eq. (10) and is

$$\begin{aligned} K_c &\equiv K(\rho_c) \\ &= (1 + 3x_c)(1 + 9x_c)a \\ &= \frac{\rho_c}{\rho_0}\left(3\frac{\rho_c}{\rho_0} - 2\right)a. \end{aligned} \quad (16)$$

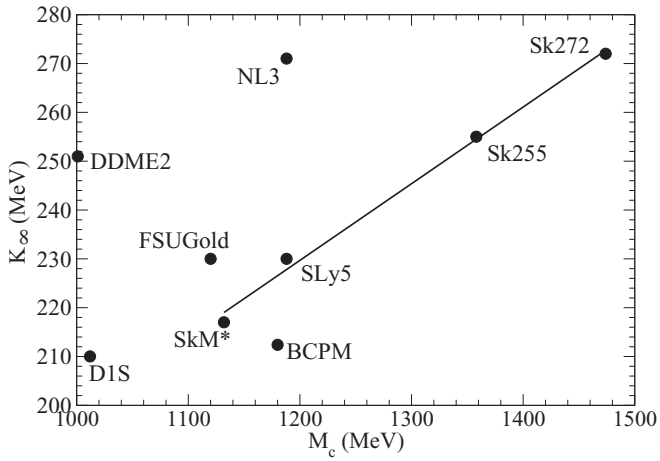

FIG. 6. K_∞ as a function of M_c for various Skyrme, Gogny, and relativistic functionals.

The value of x_c is almost identical for Skyrme and Gogny EDFs, and taking the value for a given by the linear correlation, one finds $K_c = 34 \pm 4$ MeV for Skyrme EDFs and 41 ± 4 MeV for Gogny ones, confirming the value of the crossing point shown in Table I and on Fig. 1 for the Skyrme EDFs. This approach confirms in a both quantitative and qualitative way the existence of a crossing point, especially in the case of the Skyrme and Gogny EDFs. In the case of the other EDFs, especially the relativistic ones, it is rather a crossing area that is obtained (Fig. 1), owing to the lack of a good correlation between K_∞ and Q_∞, in general; see Fig. 5. It seems therefore difficult to provide a quantitative extension of Eq. (15) beyond the Skyrme or Gogny cases.

C. Relation between K_∞ and M_c

Figure 6 displays the (M_c,K_∞) correlation for four Skyrme EDFs. Adding to this correlation graph various EDFs with other density dependencies, such as the relativistic one, drastically blurs the correlation. This originates from the large uncertainty on the value of the skewness parameter Q_∞ among the EDFs discussed in the previous section (Table III). Using Eqs. (7) and (12), the quantity M_c can be expressed as

$$M_c \simeq 3K_c + (1+3x_c)^2[9K_\infty + (1+12x_c)Q_\infty]. \quad (17)$$

The correlation between M_c and K_∞ depends on the density dependence of the binding energy reflected in the skewness parameter Q_∞, which can vary to a large extent; see Table III. More precisely, from Eq. (17), one can deduce the value of the quantity K_∞ as

$$K_\infty = \frac{1}{9}\frac{M_c - 3K_c}{(1+3x_c)^2} - \frac{1+12x_c}{9}Q_\infty, \quad (18)$$

where the first term of the right-hand side gives the dominant contribution (about 200 MeV) and the second term gives the correction (about 10 MeV) induced by the higher order density dependence, represented by the first term beyond K_∞, which is the skewness parameter Q_∞. The values of K_c and x_c are fixed by the existence of a crossing point, and M_c is extracted from the correlation analysis based on the experimental $E_{\rm GMR}$. These quantities have, however, typical uncertainties which contribute to the determination on K_∞. The uncertainty on K_c is indeed typically of about ± 5 MeV (Table I). Using Eq. (18), it provides and additional variation of K_∞ of about ± 3 MeV. The ± 100 MeV uncertainty on M_c also provides a typical ± 20 MeV uncertainty on K_∞ using Eq. (18). Now, taking a typical uncertainty for Q_∞ of ± 500 MeV (Table III), Eq. (18) provides a variation on K_∞ about ± 10 MeV, also contributing to the error bar on K_∞. It is therefore clear that the uncertainty on K_∞ is not only related to that on M_c but also related to the lack of knowledge on the density dependence of the EoS, represented in the present analysis by the skewness parameter Q_∞.

In conclusion, the relation Eq. (18) clearly shows that the uncertainty on the incompressibility modulus K_∞ is mainly related to that on the quantities M_c and Q_∞. The reduction of the error bar on K_∞ is therefore mostly related to a better knowledge of M_c, well correlated with $E_{\rm GMR}$, and of the skewness parameter Q_∞, for which new experimental constraints are found.

IV. A SIMPLE EXPRESSION RELATING $E_{\rm GMR}$ AND M_c

To provide a complementary view to microscopic approaches [1–10], it may be useful to derive an analytic relationship between the GMR centroid in nuclei and the quantity M_c, to enlighten and confirm the results obtained with a fully microscopic approach; see Sec. II and Ref. [10]. In this section we aim to derive an analytical relationship between the centroid of the GMR and the relevant quantity of the EoS, M_c defined by Eq. (7).

The energy centroid of the GMR is used to define the incompressibility in nuclei K_A [1]:

$$E_{\rm GMR} = \sqrt{\frac{\hbar^2 K_A}{m\langle r^2\rangle}}. \quad (19)$$

To derive an analytical relationship, $\langle r^2\rangle$ can be approximated by $3R^2/5$ [33], where $R \simeq 1.2A^{1/3}$ is the nuclear radius, yielding

$$E_{\rm GMR} \simeq \frac{\hbar}{R}\sqrt{\frac{5K_A}{3m}}. \quad (20)$$

We derive an analytic relation between K_A and M_c using the LDA to check, in a complementary way to microscopic approaches, the role of M_c in determining the centroid of the GMR.

The following step consists of dividing K_A into a nuclear and a Coulomb contributions, as

$$K_A = K_{\rm Nucl} + K_{\rm Coul}Z^2A^{-4/3}, \quad (21)$$

where, in the liquid drop approach, $K_{\rm Nucl}$ is defined as

$$K_{\rm Nucl} = K_\infty + K_{\rm surf}A^{-1/3} + K_\tau\left(\frac{N-Z}{A}\right)^2,$$

as in the Bethe Weissäcker formula for the binding energy [1]. The accuracy of this approach can be enhanced with the inclusion of higher order terms [34]. The quantities K_∞, $K_{\rm surf}$, and K_τ are, however, poorly constrained by the relative small data [1,35]. We prefer instead to extract $K_{\rm Nucl}$ from the LDA,

which has the advantage that (i) it was proven to be a good approximation of the microscopic calculation [12] and (ii) the consistency between the value obtained for K_A and the Skyrme functional is guaranteed.

A. The local density approximation

The nuclear contribution $K_{\rm Nucl}$ is related to the density dependence of the incompressibility $K(\rho)$ as [12],

$$K_{\rm Nucl} = \frac{\rho_0^2}{A}\int d^3r\ \frac{K[\rho(r)]}{\rho(r)}. \tag{22}$$

Equation (22) makes it possible to perform the LDA by considering the density profile of nuclei, $\rho_A(r)$, in Eq. (8), where $\rho = \rho_A(r)$. The LDA give accurate estimation of $K_{\rm Nucl}$ [12]. It should be noted that in Eq. (22), the value of $K(\rho)$ at saturation density (i.e., K_∞) does not have any specific impact on the K_A value and nor, therefore, on the prediction of $E_{\rm GMR}$. Further, owing to the existence of the crossing area $(\rho_c, K_c) \simeq (0.1\ {\rm fm}^{-3}, 35\ {\rm MeV})$, which takes into account both the Skyrme EDFs crossing (Table I) and the relativistic one (Fig. 1), $K(\rho)$ can be approximated to the first order around the crossing point by

$$K(\rho) = \frac{M_c\rho}{3\rho_c} - \frac{M_c}{3} + K_c, \tag{23}$$

where M_c is related to the first derivative of the incompressibility [Eq. (7)].

This first-order approximation is relevant as observed on the ($E_{\rm GMR}$,M_c) correlation of Figs. 2 and 3. Of course, taking the density dependence of the incompressibility as its first derivative around the crossing point remains an approximation, which explains the not-exactly linear ($E_{\rm GMR}$,M_c) correlation on Fig. 2 considering Skyrme and relativistic EDFs.

The integral in Eq. (22) is taken between $\rho_0/2$ and ρ_0, which is adapted to the linear regime around ρ_c and corresponds to the typical dispersion of the density values around the mean density in nuclei [10]. Injecting expression (23) into Eq. (22) and assuming a Fermi shape of the nuclear density, with diffusivity $\simeq$0.5 fm [33] yield the analytical relation between the centroid of the GMR and M_c, using Eqs. (20) and (21):

$$E_{\rm GMR} = \frac{\hbar}{R}\left\{\frac{20\pi}{3mA}\int_{\rho_0/2}^{\rho_0}\left[a\ln\left(\frac{\rho_0}{\rho}-1\right)+R\right]^2 \times\left(\frac{M_c\rho}{3\rho_c}-\frac{M_c}{3}+K_c\right)\frac{a}{1-\rho/\rho_0}\frac{\rho_0^2}{\rho^2}d\rho + \frac{5K_{\rm Coul}}{3m}Z^2A^{-4/3}\right\}^{1/2}. \tag{24}$$

The integral in Eq. (24) denotes the nuclear contribution, whereas the second part comes from the Coulomb effects. The Coulomb contribution is evaluated using $K_{\rm Coul} = -5.2$ MeV [1,36]. This value is obtained from the liquid drop expansion of the incompressibility and applied to several Skyrme interactions [36]. It should be noted that the Fermi shape is a good approximation of the density and we have checked that the diffusivity of the density obtained from microscopic Hartree-Fock calculations (0.47 fm) is very close to 0.5 fm. The use of the Fermi density is legitimized by the aim of tracing the analytical impact of the quantity M_c on the GMR centroid. Equation (24) also underlines the important role of the quantity M_c on the GMR centroid. On the contrary, the incompressibility at saturation density K_∞ does not play any specific role in Eq. (24). It is, therefore, rather the quantity M_c which is the relevant quantity to be constrained by the GMR measurements.

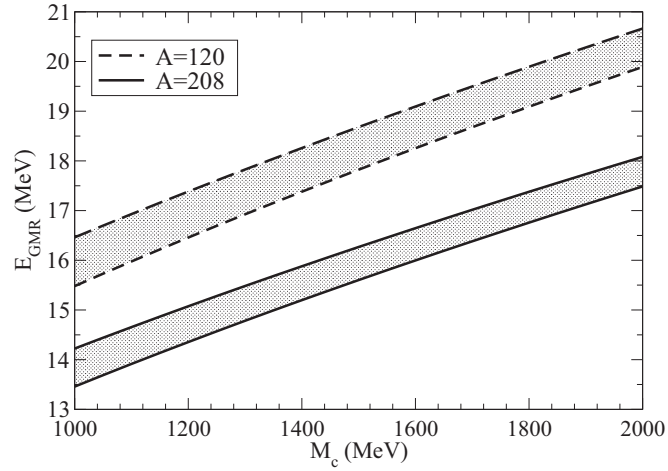

FIG. 7. Centroid of the GMR in $A = 208$ (solid lines) and $A = 120$ (dashed lines) nuclei calculated with the LDA for the nuclear incompressibility and using its first derivative at the crossing point [Eq. (24) without the Coulomb term]. The two lines for each mass number correspond to the lower and upper values of K_c deduced from its variance.

B. Results and comparison with the microscopic method

The stability of the results obtained with Eq. (24) has been studied with respect to the diffusivity value a, the LDA prescription [Eq. (22)], the crossing point (ρ_c,K_c) values, and the integration range. A sound stability is obtained against these quantities: The predicted GMR centroid does not change by more than 10% by making all these variations in relevant physical ranges. For instance, the typical variation for a given EDF between the LDA value of K_A and the microscopic one is of 7%, except in the DDME2 case, where the linear approximation Eq. (23) is less suited (15% variation on K_A).

We first study the behavior of the nuclear contribution [$K_{\rm Coul} = 0$ in Eq. (24)]. Figure 7 displays the correlation between the centroid of the GMR and the M_c value using Eq. (24), for nuclei with $A = 208$ and $A = 120$. For each mass number the values obtained with the lower and upper values of K_c (see Table I) are displayed. A good qualitative agreement is obtained with the fully microscopic results (see Fig. 2 and 3) in view of the approximations performed to derive Eq. (24). The A dependence is also well described. These results confirm the validity of the present approach and emphasize M_c as a relevant EoS quantity to be constrained by the GMR measurements. It also qualitatively agrees with the microscopic results.

To perform a more quantitative study, the curves on Fig. 8 display the centroid of the GMR in ^{208}Pb and ^{120}Sn nuclei predicted using the full Eq. (24) with both the nuclear and the

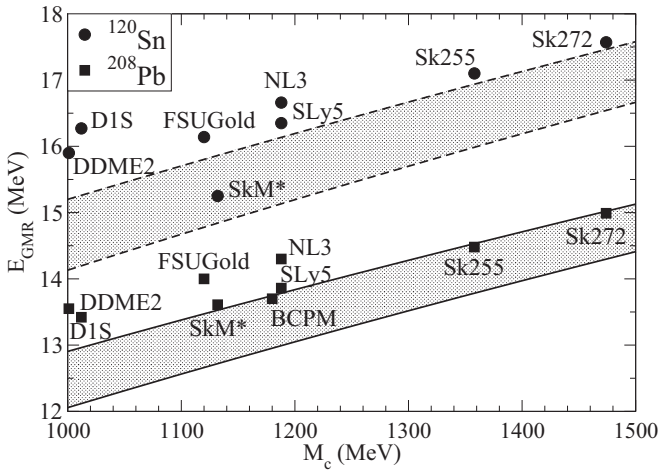

FIG. 8. Centroid of the GMR in ^{208}Pb (solid lines) and ^{120}Sn (dashed lines) calculated with the LDA and including the Coulomb effects as a function of M_c. The two lines for each mass number correspond to the lower and upper values of K_c deduced from its variance. The values for various EDF obtained microscopically (squares and dots) are also displayed for comparison.

Coulomb contributions. The comparison with the microscopic results using various EDFs is also shown. A good agreement is obtained in both cases, strengthening again the present analytical LDA approach, and emphasizing the role of M_c. Comparing Figs. 7 and 8, the Coulomb effect on the GMR centroid can be evaluated to be about 1 MeV in heavy nuclei.

The remaining small underestimation of the data by the present LDA approach might indicate the need for possible ameliorations. For instance, the contribution of the gradient terms in the LDA, neglected in the present analysis, could be further included within the improved Thomas-Fermi approximation in Eq. (22) [37]. We have also checked that a different value of $K_{\rm Coul}$ (-3 MeV) also contributes to an improved description of the data. A better understanding of the respective contributions of the gradient terms and the Coulomb one in the LDA is a relevant path to further investigate within the improved Thomas Fermi approach.

The almost linear correlation between $E_{\rm GMR}$ and M_c observed on Fig. 8 can be further investigated. Equation (24) can be rewritten as

$$E_{\rm GMR} = [\alpha(A,\rho_0)M_c + \beta(A,Z,\rho_0)]^{1/2}, \tag{25}$$

with

$$\alpha(A,\rho_0) \equiv \frac{20\pi\hbar^2}{9mAR^2}\int_{\rho_{\rm min}}^{\rho_0}\left[a\ln\left(\frac{\rho_0}{\rho}-1\right)+R\right]^2 \times\left(\frac{\rho}{\rho_c}-1\right)\frac{a}{1-\rho/\rho_0}\frac{\rho_0^2}{\rho^2}d\rho, \tag{26}$$

$$\beta(A,Z,\rho_0) \equiv \frac{5\hbar^2 K_{\rm Coul}}{3mR^2}Z^2A^{-4/3} + \frac{20\pi\hbar^2}{3mAR^2} \times\int_{\rho_{\rm min}}^{\rho_0}\left[a\ln\left(\frac{\rho_0}{\rho}-1\right)+R\right]^2\frac{aK_c}{1-\rho/\rho_0}\frac{\rho_0^2}{\rho^2}d\rho. \tag{27}$$

Fixing ρ_c and K_c, the coefficients α and β only depend on the nucleus' mass and charge (A, Z), and on the saturation density ρ_0, which is constrained by the charge radii. Typical values are $\alpha = 0.12$ MeV and $\beta = 42$ MeV^2 in the case of ^{208}Pb and $\alpha = 0.16$ MeV and $\beta = 75$ MeV^2 in the case of ^{120}Sn.

It should be noted that the LDA approximation (25) of $E_{\rm GMR}$ can be obtained because of the existence of the crossing point. In Eq. (25), the energy of the GMR depends on the functional mostly through the parameter M_c. In conclusion, the LDA makes it possible to obtain expression (25) relating $E_{\rm GMR}$ with M_c in a simple and accurate form.

Introducing (M_0,E_0) as the reference point, where $M_0 \equiv$ 1200 MeV and E_0 is the corresponding GMR energy, one can go one step further and linearize Eq. (25) with respect to $M_c - M_0$, as

$$E_{\rm GMR} \simeq \frac{\alpha}{2E_0}M_c + \left(E_0 - \frac{\alpha M_0}{2E_0}\right). \tag{28}$$

This is justified for the typical values of M_c, ranging between 1000 and 1500 MeV, as shown on Fig. 8. The almost linear correlation between $E_{\rm GMR}$ and M_c observed on Fig. 8 is therefore understood by the present approach [Eq. (28)]. It clearly shows that the measurement of the GMR position constrains M_c, which is a first information on the density dependence of the incompressibility. It should be recalled that such a quantitative description is not possible with K_∞ because there is no crossing point of the incompressibility at saturation density: Equation (24) is not applicable in that case.

V. CONCLUSIONS

The relationship between the isoscalar GMR and the EoS raises the question of which EoS quantity is constrained by GMR centroid measurements. The incompressibility modulus K_∞ alone may not be the relevant one nor the most direct because the more general density dependence of the incompressibility should be considered. A crossing area is observed on $K(\rho)$ at $\rho_c \simeq 0.1$ fm^{-3} among various functionals. Using a microscopic approach, such as constrained HFB, the slope M_c of $K(\rho)$ at the crossing density can be directly constrained by GMR measurements. This assesses the change of the method in extracting EoS quantities from GMR: M_c is first constrained, and an approximate value of K_∞ can be deduced in a second step [10].

The stability of K_c has been demonstrated in the case of Skyrme EDFs. A general relationship between M_c and K_∞ is obtained, showing the contribution of the uncertainty in the density dependence of the EoS which has been cast into the quantities Q_∞. The K_∞ value can be determined in a second step from the knowledge of the M_c value, requiring a better constraint on the skewness parameter Q_∞, being one of the main uncertainties for the density dependence of the incompressibility between the crossing density and the saturation density. One should recall that the K_∞ value remains 230 ± 40 MeV (17% uncertainty), whereas the quantity M_c is better constrained to be $M_c \simeq 1050 \pm 100$ MeV (9% uncertainty) [10]. A better

knowledge of higher order density-dependent terms of $E/A(\rho)$, e.g., the skewness parameter Q_∞, shall help to more accurately relate the parameter M_c to the incompressibility modulus K_∞.

Using the LDA approach and an analytical approximation of the density, the microscopic results have been confirmed: The measurement of the centroid of the isoscalar GMR constrains the first derivative M_c of the incompressibility around the crossing point $\rho_c \simeq 0.1\,\mathrm{fm}^{-3}$. An analytical relation between the centroid of the GMR and the quantity M_c is derived and the predicted GMR centroid is found, in agreement with the microscopic method.

ACKNOWLEDGMENTS

The authors thank I. Vidaña for fruitful discussions. This work has been partly supported by Contract No. ANR SN2NS, the Institut Universitaire de France, and by CompStar, a Research Networking Programme of the European Science Foundation.

[1] J.-P. Blaizot, Phys. Rep. **64**, 171 (1980).
[2] D. Vretenar, T. Niksic, and P. Ring, Phys. Rev. C **68**, 024310 (2003).
[3] B. K. Agrawal, S. Shlomo, and V. Kim Au, Phys. Rev. C **68**, 031304(R) (2003).
[4] G. Colo, N. V. Giai, J. Meyer, K. Bennaceur, and P. Bonche, Phys. Rev. C **70**, 024307 (2004).
[5] J. Piekarewicz, Phys. Rev. C **76**, 031301(R) (2007).
[6] T. Li *et al.*, Phys. Rev. Lett. **99**, 162503 (2007).
[7] J. Li, G. Colò, and J. Meng, Phys. Rev. C **78**, 064304 (2008).
[8] E. Khan, Phys. Rev. C **80**, 011307(R) (2009).
[9] P. Veselý, J. Toivanen, B. G. Carlsson, J. Dobaczewski, N. Michel, and A. Pastore, Phys. Rev. C **86**, 024303 (2012).
[10] E. Khan, J. Margueron, and I. Vidaña, Phys. Rev. Lett. **109**, 092501 (2012).
[11] O. Civitarese, A. G. Dumrauf, M. Reboiro, P. Ring, and M. M. Sharma, Phys. Rev. C **43**, 2622 (1991).
[12] E. Khan, J. Margueron, G. Colò, K. Hagino, and H. Sagawa, Phys. Rev. C **82**, 024322 (2010).
[13] Li-Gang Cao, H. Sagawa, and G. Colò, Phys. Rev. C **86**, 054313 (2012).
[14] N. Paar, D. Vretenar, E. Khan, and G. Colò, Rep. Prog. Phys. **70**, 691 (2007).
[15] D. J. Thouless, Nucl. Phys. **22**, 78 (1961).
[16] O. Bohigas, A. M. Lane, and J. Martorell, Phys. Rep. **51**, 267 (1979).
[17] L. Capelli, G. Colò, and J. Li, Phys. Rev. C **79**, 054329 (2009).
[18] A. L. Fetter and J. D. Walecka, *Quantum Theory of Many-Particle Systems* (McGraw-Hill, New York, 1971).
[19] J. Piekarewicz, Phys. Rev. C **83**, 034319 (2011).
[20] B. A. Brown, Phys. Rev. Lett. **85**, 5296 (2000).
[21] S. Typel and B. A. Brown, Phys. Rev. C **64**, 027302 (2001).
[22] E. Khan, M. Grasso, and J. Margueron, Phys. Rev. C **80**, 044328 (2009).
[23] C. Horowitz, Z. Ahmed, C.-M. Jen *et al.*, Phys. Rev. C **85**, 032501 (2012).
[24] M. Baldo, L. M. Robledo, P. Schuck, and X. Viñas, Phys. Rev. C **87**, 064305 (2013)
[25] G. A. Lalazissis, J. Konig, and P. Ring, Phys. Rev. C **55**, 540 (1997).
[26] G. A. Lalazissis, T. Niksic, D. Vretenar, and P. Ring, Phys. Rev. C **71**, 024312 (2005).
[27] J. Bartel, P. Quentin, M. Brack, C. Guet, and H.-B. Hakansson, Nucl. Phys. A **386**, 79 (1982).
[28] J. F. Berger, M. Girod, and D. Gogny, Comp. Phys. Comm. **63**, 365 (1991).
[29] E. Chabanat, P. Bonche, P. Haensel, J. Meyer, and R. Schaeffer, Nucl. Phys. A **635**, 231 (1998).
[30] C. Ducoin, J. Margueron, and C. Providência, Europhys. Lett. **91**, 32001 (2010).
[31] C. Ducoin, J. Margueron, C. Providência, and I. Vidaña, Phys. Rev. C **83**, 045810 (2011).
[32] J. P. Blaizot, J. F. Berger, J. Dechargé, and M. Girod, Nucl. Phys. A **591**, 435 (1995).
[33] P. Ring and P. Schuck, *The Nuclear Many-Body Problem* (Springer-Verlag, Heidelberg, 1980).
[34] S. K. Patra, M. Centelles, X. Viñas, and M. Del Estal, Phys. Rev. C **65**, 044304 (2002).
[35] J. M. Pearson, N. Chamel, and S. Goriely, Phys. Rev. C **82**, 037301 (2010).
[36] H. Sagawa, S. Yoshida, G.-M. Zeng, J.-Z. Gu, and X.-Z. Zhang, Phys. Rev. C **76**, 034327 (2007).
[37] M. Brack, C. Guet, and H.-B. Håkansson, Phys. Rep. **123**, 275 (1985).